Title: Structural insights reveal the second base catalyst of isomaltose glucohydrolase

Authors: Takayoshi Tagami[1], Minghao Chen[2], Yuta Furunaga[1], Asako Kikuchi[1], Juri Sadahiro[1], Weeranuch Lang[1], Masayuki Okuyama[1], Yoshikazu Tanaka[2, 3, *], Tomohito Iwasaki[4], Min Yao[2, 3], and Atsuo Kimura[1]

[1]Resarch Faculty of Agriculture, Hokkaido University, Sapporo 060-8589, Japan

[2]Graduate School of Life Science, Hokkaido University, Sapporo 060-0810, Japan

[3]Faculty of Advanced Life Science, Hokkaido University, Sapporo 060-0810, Japan

[4]College of Agriculture, Food and Environment Sciences, Rakuno Gakuen University, Ebetsu 069-8501, Japan

*Present affiliation: Graduate School of Life Sciences, Tohoku University, Sendai 980-8577, Japan

Correspondence:

T. Tagami: Research Faculty of Agriculture, Hokkaido University, Kita-9 Nishi-9 Kitaku, Sapporo, Hokkaido 060-8589, Japan; Tel: +81-11-706-2816; E-mail: tagami@abs.agr.hokudai.ac.jp

M. Yao: Graduate School of Life Science and Faculty of Advanced Life Science, Hokkaido University, Kita-10 Nishi-8 Kitaku, Sapporo, Hokkaido 060-0810, Japan; Tel: +81-11-706-4479; E-mail: yao@castor.sci.hokudai.ac.jp

A. Kimura: Research Faculty of Agriculture, Hokkaido University, Kita-9 Nishi-9 Kitaku, Sapporo, Hokkaido 060-8589, Japan; Tel: +81-11-706-2808; E-mail: kimura@abs.agr.hokudai.ac.jp

Running title: Second base catalyst of isomaltose glucohydrolase

Abbreviations: GAMase, glucoamylases; GDXase, glucodextranase; GH, glycoside hydrolase family; IGHase, isomaltose glucohydrolase; native SAD, single-wavelength anomalous dispersion method using sulfur atoms; WT, wild-type IGHase.

Keywords: Glycoside hydrolase; Kinetic analysis; pH-activity profile; Condensation; Native SAD

Conflicts of interests: The authors declare no competing interests.

Data accessibility

The atomic coordinates and structure factors of IGHase derivatives have been deposited into PDB with accession code 5Z3A, 5Z3B, 5Z3C, 5Z3D, 5Z3E, 5Z3F, 7C24, 7C25, 7C26, and 7C27.

Abstract

Glycoside hydrolase family 15 (GH15) inverting enzymes contain two glutamate residues functioning as a general acid catalyst and a general base catalyst, for isomaltose glucohydrolase (IGHase), Glu178 and Glu335, respectively. Generally, a two catalytic residue-mediated reaction exhibits a typical bell-shaped pH-activity curve. However, IGHase is found to display atypical non-bell-shaped pH-k_{cat} and pH-k_{cat}/K_m profiles, theoretically better-fitted to a three catalytic residue-associated pH-activity curve. We determined the crystal structure of IGHase by the single-wavelength anomalous dispersion method using sulfur atoms and the cocrystal structure of a catalytic base mutant E335A with isomaltose. Although the activity of E335A was undetectable, the electron density observed in its active site pocket did not correspond to an isomaltose but a glycerol and a β-glucose, cryoprotectant and hydrolysis product, respectively. Our structural and biochemical analyses of several mutant enzymes suggest that Tyr48 acts as a second catalytic base catalyst. Y48F mutant displayed almost equivalent specific activity to a catalytic acid mutant E178A. Tyr48, highly conserved in all GH15 members, is fixed by another Tyr residue in many GH15 enzymes; the latter Tyr is replaced by Phe290 in IGHase. The pH profile of F290Y mutant changed to a bell-shaped curve, suggesting that Phe290 is a key residue distinguishing Tyr48 of IGHase from other GH15 members. Furthermore, F290Y is found to accelerate the condensation of isomaltose from glucose by modifying a hydrogen-bonding network between Tyr290-Tyr48-Glu335. The present study indicates that the atypical Phe290 makes Tyr48 of IGHase unique among GH15 enzymes.

Introduction

Almost all organisms obtain energy from monosaccharides. For instance, glucose can be produced from starch and glycogen by amylolytic enzymes [1], followed by glycolysis pathway. On the other hand, eukaryotic cells control the quality of proteins with removing the two outermost glucose residues of *N*-glycans using glycan-processing enzymes [2,3]. Thus, the glycoside hydrolases, which catalyze the hydrolysis of glycosidic bonds in complex sugars, are one of the most biologically important catalysts. Additionally, many glycosidases are important industrially as well. For example, cellulolytic enzymes play the critical roles in the saccharification of plant biomass for biofuel production [4], and glycosidases with high transglycosylation activity, e.g., some α-glucosidases [5–8], are used for producing important oligosaccharides, such as isomaltose, on a commercial scale. Therefore, gaining insights into the molecular mechanisms of glycoside hydrolases will enable us to develop effective inhibitors [9], engineer a hydrolase into a glycosynthase [10], and other applications.

Henrissat and colleagues have classified the glycoside hydrolases into 171 families based on their sequence similarities [11]. The enzymes belonging to the same glycoside hydrolase family (GH) are believed to share the same three-dimensional structures and catalytic mechanisms. GH15 was one of the first established GH groups, and five fungal glucoamylases (GAMase; EC 3.2.1.3) were classified into GH15 at the time of establishment [12]. Thereafter, glucodextranase (GDXase; EC 3.2.1.70) [13], α,α-trehalase (EC 3.2.1.28) [14,15], and dextran dextrinase (EC 2.4.1.2) and its related enzyme [16,17] were categorized into this family, and isomaltose glucohydrolase (IGHase; EC 3.2.1.205) [18] was found most recently.

GH15 enzymes hydrolyze α-glucosidic linkages at the non-reducing ends to release β-glucose; that is, they hydrolyze substrates with a net inversion of anomeric configuration. Hiromi et al. [19,20] first reported that, based on the kinetic analysis, two carboxy groups were involved in the catalysis by GAMase, which showed a typical bell-shaped pH-hydrolysis velocity profile. Svensson and colleagues [21] found three candidates for the catalytic residues of GAMase based on labeling experiments. These observations were confirmed by the crystal structures of GAMase by Aleshin, Harris, and colleagues [22–24], which revealed that the enzyme had a catalytic $(\alpha/\alpha)_6$-barrel domain bearing two glutamate residues in the loopα5→α6 and loopα11→α12 that acted as a catalytic acid and base, respectively. A water molecule trapped by the base residue is the attacking nucleophile in hydrolysis. This reaction mechanism is known to be a single-displacement mechanism involving an oxocarbenium ion-like transition state [25]. The two glutamate residues are completely conserved among all the GH15 enzymes; thus, it is believed that all the GH15

hydrolases achieve hydrolysis *via* the single-displacement mechanism, despite their different substrate specificities.

IGHase has been identified as a member of the catabolic enzymes of cyclobis-(1→6)-α-nigerosyl, a cyclic glucotetraose with alternate α-1,6- and α-1,3-glucosidic linkages, from the actinobacterium *Kribbella flavida* NBRC 14399 [18]. IGHase specifically hydrolyzes the α-1,6-glucosidic linkage in isomaltose with the release of β-glucose. The substitutions of Glu178 and Glu335, the predicted general acid and general base residues of IGHase, respectively, result in a significant decrease or complete loss of activity, suggesting that IGHase follows the same two-glutamate-dependent single-displacement mechanism as other GH15 enzymes. Recently, however, we found that IGHase exhibited a unique pH-hydrolysis velocity profile that indicates a three-residue-dependent hydrolysis reaction. This report provides structural and kinetical evidence that a tyrosine residue, as a second catalytic base residue, is responsible for the hydrolysis reaction of IGHase.

Results

IGHase displays an atypical pH-hydrolysis velocity profile. We estimated the kinetic parameters, k_{cat} and K_m, of the wild-type IGHase (WT) for isomaltose hydrolysis at various pHs (Table 1). All the s vs. $v/[E]_0$ plots (except at pH 4.2) fit the Michaelis-Menten equation well, and the k_{cat} and K_m values were determined. The apparent k_{cat}/K_m value at pH 4.2 was obtained from the slope of the $1/s$ vs. $[E]_0/v$ plots. Both the pH vs. k_{cat} plots and pH vs. k_{cat}/K_m plots did not show the typical bell shape but a tailed shape instead (Figure 1A). Thus, we proposed a three-residue-dependent hydrolytic process to describe the tailed curves (Scheme 2 in Figure 1B). In this process, there are three catalytic ionizable groups with ionization constants K_{e1}, K_{e2}, and K_{e3}, respectively. The enzyme forms a Michaelis complex with the substrate in all protonation states, EH3, EH2, EH, and E, with the respective dissociation constants, K_{s1}, K_{s2}, K_{s3}, and K_{s4}. However, only two states, EH2S and EHS, are reactive with a rate constant, k_1 and k_2, respectively. The k_{cat} and k_{cat}/K_m values in this process are described by Eqs. 3 and 4 (see Methods). In addition, the pH vs. k_{cat} plots and pH vs. k_{cat}/K_m plots fit the regression curves of the three-residue-dependent hydrolysis process better than the bell-shaped curves (Eqs. 1 and 2) [26] that describes a two-residue-dependent hydrolytic process. Finally, the values of pK_{e1}, pK_{e2}, and pK_{e3} were determined to be 5.0, 6.6, and 8.3, respectively, and the value of k_1/K_{s2} (25 s^{-1} mM^{-1}) was higher than that of k_2/K_{s3} (8.5 s^{-1} mM^{-1}) (Table 2).

Catalytic-base mutant enzyme of IGHase hydrolyzed isomaltose in the crystal. We first tried to determine the crystal structure of IGHase with a molecular replacement method

using the structures of the other GH15 enzymes as search models (PDB: 1GAI, 2FBA, and 1LF6) having 19-23% sequence identities; however, we were unable to obtain any reasonable phase information. Therefore, the structure of IGHase was determined by the single-wavelength anomalous dispersion method using sulfur atoms (native SAD) as scattering factors at 2.5 Å resolution (Table 3). Subsequently, we used the molecular replacement approach to determine the high-resolution crystal structures of WT, E178A and E335A (the former, a catalytic-acid mutant; the latter, a catalytic-base mutant) at 1.4, 1.6, and 1.1 Å, respectively (Table 4).

All of the structures displayed an almost identical overall structure with root mean square deviations of 0.2 Å (E335A) and 0.1 Å (E178A) from the WT, as calculated by the DALI pairwise server [27]. IGHase is a single-domain protein with an $(\alpha/\alpha)_6$-barrel fold and an α-helix insertion between the 11th and 12th α-helices of the barrel fold (Figure 2A). The extra α-helix is atypical in the GH15 enzymes (Figure 2B), likely contributing to the critical function of IGHase during isomaltose hydrolysis as discussed below. One of two glycerol molecules derived from the cryoprotectant was observed at subsite −1 at the same conformation in the three crystal structures, and another glycerol molecule existed at subsite +1 in the WT structure; "subsite" is a substrate-binding site that recognizes a monosaccharide moiety [28]. The catalytic acid and catalytic base residues, Glu178 and Glu335, were located in the loopα5→α6 and loopα11→α12 in the $(\alpha/\alpha)_6$-barrel fold, respectively, as in the other GH15 enzymes.

The cocrystal structure of E335A with isomaltose was determined at 1.1 Å resolution. Although the hydrolytic activity of E335A was undetectable (Table 5) [18], the electron density observed in its active site pocket did not correspond to an isomaltose but a glycerol (cryoprotectant) and a β-glucose, the product of the hydrolysis (Figure 3A). The β-glucose at subsite −1 was held by hydrogen bonds and van der Waals interactions. Specifically, the side chains of Tyr48, Arg55, Asp56, and Arg284 and the main-chain carbonyl group of Trp176 formed hydrogen bonds with the hydroxy groups of the glucose. Notably, the hydroxy group of Tyr48 was located at 2.8 and 3.5 Å from the O1 and O5 of the β-glucose, respectively. Meanwhile, Trp296, Leu298, Leu361, and Trp363 were located at the bottom of the active pocket, where Ala41 and Trp53 formed hydrophobic patches to accommodate the C6 of the glucose. The subsite +1 occupied by the glycerol molecule was formed by Glu179, whose side chain turned in an opposite direction to that of the catalytic acid Glu178, Phe290 in the loopα9→α10 of the barrel, and Trp350 and Trp354 in the extra α-helix. A docking simulation of isomaltose to WT suggested that the hydroxy groups of the isomaltose molecule were held at almost the same positions as those of the β-glucose and glycerol observed in the E335A complex with the highest affinity of −8.7 kcal/mol (Figure 3B). The reducing glucose moiety

of isomaltose at subsite +1 seemed to form hydrogen bonds at the O4 and O3 with the side chains of Arg284 and Glu179, respectively, and edge-to-face interactions with the bulky side chains of Phe290, Trp350, and Trp354. The hydroxy group of Tyr48 was located at 3.1 Å from both the O5 of the non-reducing glucose and the Oε2 of Glu335. The Oε1 of Glu178 was located 4.7 Å from the glucosidic oxygen of isomaltose.

All active site residues except Phe290, Trp350 and Trp354 of IGHase were located in the conserved regions S1 and S3–5 in the catalytic domains of GH15 [29] and completely conserved in GH15 enzymes for which three-dimensional structures have been determined (Figure 3C). Meanwhile, WT shared the spatially homologous Trp350 or the conformationally homologous Phe290 with these GH15 members (Figure 3D). The spatial arrangement of Trp350 is similar to Trp582 in *Arthrobacter globiformis* GDXase, which is considered one of the key residues responsible for the enzyme's high specificity for α-1,6-glucan [13]. The position corresponding to Phe290 is highly conserved as a Tyr residue in the other GH15 enzymes. In the other GH15 structures, this Tyr residue forms a hydrogen bond to the Tyr corresponding to Tyr48 of IGHase.

Trp350, Trp354, Phe290 and Tyr48 play important roles in IGHase activity. Enzyme variants with mutations at the active site residues were characterized (Table 5). W350A and W354A displayed 25- and 48-fold lower k_{cat} values and 5.4- and 3.3-fold higher K_m values for isomaltose hydrolysis than the WT; however, these mutant enzymes and WT displayed the highest substrate specificity for isomaltose (Table 6). In addition, W354A hydrolyzed all of the α-glucobioses, of which maltose, nigerose, and trehalose were not hydrolyzed by WT.

F290Y exhibited almost the same specific activity, kinetic parameters, and substrate specificity as WT (Table 5 and 6). However, the pH profiles of the k_{cat} and k_{cat}/K_m of F290Y were different from those of WT. The pH-k_{cat}/K_m plots fit the bell-shaped curve well (Table 1 and Figure 1A). The values of pK_{e1} and pK_{e2} were determined to be 4.8 and 7.4, respectively (Table 2). When the three-residue-dependent hydrolytic process was applied to the regression analysis, pK_{e1}, pK_{e2} and pK_{e3} were estimated to be 4.6, 4.5 and 7.4, respectively (Table 2), at which both pK_{e1} and pK_{e2} shared almost identical values. F290Y had almost the same overall structure and conformations of the active pocket residues, including the glycerol at subsite −1, as WT (Figure 4A). The hydroxy group of the introduced Tyr290 formed a hydrogen-bonding network with Tyr48 and Glu335, as observed in the other GH15 enzymes.

On the other hand, Y48F displayed almost no activity (Table 5). Its specific activity was 0.00566 U/mg, almost equivalent to that of E178A, which is a general-acid mutant. It was impossible to determine the pH profile and substrate specificity of Y48F due to its extremely low activity. With a glycerol molecule at subsite −1, the overall crystal structure of Y48F was

almost identical to that of WT (Figure 4B). The side chain of Phe48 slightly swung from that of Tyr48 of WT, even though the conformations of the other active site residues were the same as WT. Such movement of Tyr48 away from Glu335 was also observed in the crystal structures of E335A and its complex with β-glucose (Figure 4C and 4D), indicating that Tyr(Phe)48 moved without the attraction between the hydroxy group of Tyr48 and the carboxy group of Glu335. The docking simulation of Y48F and isomaltose suggested that Y48F was bound to isomaltose in the same manner as WT with the same affinity at −8.7 kcal/mol (Figure 5).

Substitution of Phe290 by Tyr accelerated condensation. The WT, Y48F, and F290Y were reacted with 1 M glucose, and the resultant condensation product was analyzed using TLC and high-performance anion-exchange chromatography with a pulsed amperometric detector. Although no product was observed in the reaction with Y48F, WT and F290Y catalyzed condensation to generate isomaltose (Figure 6A). The progress curves (time *versus* [isomaltose]) of their condensation reactions reached a plateau (Figure 6B), indicating that the reactions reached an equilibrium between condensation (glucose to isomaltose) and hydrolysis (isomaltose to glucose). F290Y was a more efficient catalyst for condensation than WT since F290Y could shorten the time needed to reach equilibrium.

Discussion

It has been believed that all GH15 enzymes have two catalytic glutamate residues and display typical bell-shaped pH vs. k_{cat}/K_m plots. However, our present study reveals that IGHase shows the non-bell-shaped pH vs. k_{cat} plots and pH vs. k_{cat}/K_m plots. Brocklehurst and Dixon demonstrated that pH-k_{cat}/K_m profiles of Scheme 1 (Figure 1B), for some cases, do not need to be symmetrical bell-shaped curves [26]. However, Scheme 1 cannot explain the non-bell-shaped pH-k_{cat} profile of IGHase; therefore, we proposed the three-residue-dependent hydrolytic process (Scheme 2 in Figure 1B) accounting for both the pH vs. k_{cat} plots and pH vs. k_{cat}/K_m plots (Figure 1A). Scheme 2, generating the product from EH2S and EHS, aligns favorably with the atypical pH-k_{cat} of WT. At decreasing pH, a main component becomes EH2S, whose k_1 (16 s^{-1}) is lower than k_2 (29 s^{-1} for EHS), forming a curve with a shoulder.

The substitution of Tyr48 with Phe in the Y48F mutant drastically decreased the specific activity of IGHase to a level comparable to that of the catalytic-acid mutant E178A. Y48F was estimated to have the same affinity for isomaltose as WT by the docking simulation analysis, indicating that the hydroxy group of Tyr48 had little contribution to the trapping of the substrate. Furthermore, the crystal structures revealed that Tyr48 of IGHase formed

hydrogen bonds with the catalytic base residue and the glucose not at subsite +1 but at subsite −1, which was observed in E335A-Glc complex and the docking models with isomaltose (Figure 3 and 5); these results suggest that Tyr48 is a catalytically essential residue. Moreover, these results indicate that the unusual pH-activity profile of IGHase is attributed to the high dependency of its catalytic efficiency on the ionization state of Tyr48 in addition to the catalytic acid Glu178 and catalytic base Glu335. Furthermore, these results suggest that the hydroxy group of Tyr48 significantly contributes to the cleavage of glucosidic linkage rather than the trapping of the substrate by the hydrogen bond.

McIntosh et al. reported that the apparent pK_a values of the catalytic residues obtained from the pH vs. k_{cat}/K_m plots agreed well with those measured by NMR in *Bacillus circulans* xylanase [30]. Here according to the regression analysis of the pH profile of IGHase using Scheme 2, pK_{e1} and pK_{e2} likely represent the pK_a of Glu335 and Tyr48, respectively, and k_1/K_{s2} and k_2/K_{s3} likely represent the catalytic efficiencies of IGHase under the protonated and deprotonated conditions of Tyr48, respectively. Therefore, the catalytic residues of EH2 are composed of Glu178-COOH (acid), Glu335-COO^- (base), and Tyr48-OH (base stabilizer). The protonation states of EH are also identical to those of EH2 except Tyr48-O^- (base). The estimated pK_a of Tyr48 (pH 6.6) was smaller than an average value around pH 10. On the other hand, Withers *et al*., reported that the phenolic oxygen of Tyr at a proper distance from Glu or Asp residue achieves appreciable negative ion character [31]. In the case of WT IGHase, the hydroxy group of Tyr48 appears to interact with only substrate and the carboxy group of Glu335, implying that Glu335 lowers pK_a of Tyr48. On the other hand, the crystal structure of E335A showed that the hydroxy group of Tyr48 formed a water-mediated hydrogen bond with the catalytic acid Glu178, thus Glu178 might lower pK_a of Tyr48 in the case of E335A. In fact, we determined the crystal structures of WT and F290Y at pH 4.5 and 8.0, but their structures were almost identical to those at pH 6.1 (Table 7 and Figure 7A). In particular, no spatial difference was observed at Glu178, Glu335 or Tyr48 (Figure 7B), indicating that Tyr48-OH and Tyr48-O^- interacted with the same chemical groups of the residues or carbohydrate ligands in the catalytic site.

Tyr48 is the only amino acid displaying a direct interaction with Glu335 of catalytic base and a catalytic water. Isomaltose hydrolysis in the EH2S process may occur as follows (Figure 8A): the hydrogen atom of Tyr48-OH interacts with the deprotonated carboxy (-COO^-) of Glu335, which removes a proton of catalytic water, in the Michaelis complex, and after completing the hydrolysis of isomaltose, the polarized oxygen atom of Tyr48-OH forms a hydrogen bond with the hydrogen of Glu335-COOH. In EHS-associated hydrolysis (Figure 8B), there are two possibilities: (i) the carboxy of Glu335 or (ii) the negative-charged oxygen of Tyr48 (-O^-) may draw a proton of the catalytic water; in the latter case, Tyr48 acts as a

catalytic base to activate the catalytic water. After hydrolysis is completed, Glu335 and Tyr48 forms a hydrogen bond in both cases.

Our proposed mechanisms are supported by structural analysis and kinetic experiments. The hydrolysis of isomaltose that occurred in the cocrystals of E335A and isomaltose might be catalyzed by the deprotonated Tyr48 as the general base. The value of k_1/K_{s2} (25 s^{-1} mM^{-1}; EH2) was higher than that of k_2/K_{s3} (8.5 s^{-1} mM^{-1}; EH), indicating that the protonated Tyr48 of EH2 was more favorable for isomaltose hydrolysis than the deprotonated form of EH. The hydrogen atom and the electron-rich oxygen atom of the hydroxy group of Tyr48 can stabilize the negatively charged side chain of Glu335 and the cationic oxocarbenium ion-like transition state, respectively. On the other hand, a deprotonated Tyr48 of EH may accompany the possible electrostatic negative-charge repulsion with deprotonated Glu335, creating a disadvantage for isomaltose hydrolysis and yielding a smaller k_2/K_{s3}.

The position of Tyr48 of IGHase is highly conserved in GH15 enzymes. Frandsen, Nerinckx, and their colleagues suggested that this Tyr residue is important in GAMase for maintaining the active site geometry and for stabilizing the oxocarbenium ion-like transition state [32,33]. However, the substitution of Tyr48 with Trp in *Aspergillus niger* GAMase is not lethal since the mutant enzyme retained approximately 1% of the k_{cat} and k_{cat}/K_m values of the wild-type enzyme [32], indicating that the degrees of dependence of the catalytic base residue on Tyr48 are different between GAMase and IGHase.

GAMase from *Aspergillus awamori* forms an intricate hydrogen-bonding network around the catalytic base residue (Glu400) with Tyr48, Tyr311, Asn315, Gln401, and Ser411 [32]. Tyr48 and Tyr311 are completely conserved in GAMase and GDXase, but Tyr311 is substituted by Phe290 in IGHase (Figure 3D). The F290Y of IGHase form a hydrogen-bonding network with Tyr48, Tyr290, and Glu335 (Figure 4A), and the pH profile of F290Y resembled a bell shape (Figure 1A). These results indicate that Glu335 and Tyr48 in F290Y work cooperatively almost as one general base residue as in the other GH15 enzymes.

One example of this three-residue-cooperativity is the F290Y-catalyzed condensation. Most hydrolases, including glycosylases, perform condensation, a reverse reaction of hydrolysis. The hydrolysis reaction involving elementary reaction intermediates (I) is as follows:

Substrate $\rightarrow I_1 \rightarrow I_2 \rightarrow \rightarrow \rightarrow I_{n-1} \rightarrow I_n \rightarrow$ Product.

Conversely, the condensation reaction involving intermediates is as follows:

Product $\rightarrow I_n \rightarrow I_{n-1} \rightarrow \rightarrow \rightarrow I_2 \rightarrow I_1 \rightarrow$ Substrate.

Therefore, the reaction mechanism of condensation should follow the reverse-manner of hydrolysis. First, IGHase initiates condensation by binding two glucose molecules to subsites −1 and +1 separately, and β-glucose should bind to the −1 subsite. Then, IGHase terminates

the reaction by the formation of isomaltose and H_2O. Glu178 acts as a general base to remove a hydrogen atom of the hydroxy group of glucose at subsite +1, and Glu335 or Tyr48 acts as a general acid to add a proton to C1-OH of the β-glucose. Interestingly, F290Y allowed its condensation to reach equilibrium much more quickly than WT (Figure 6B), likely due to the anion resonance stabilization among Glu335, Tyr48, Tyr290, and bulk waters (Figure 8C). Glu335-OH or Tyr48-OH may provide a proton to the oxygen atom of C1-OH in β-glucose in a condensation reaction; however, these residues tend to be deprotonated due to their low pK_a values in WT bearing Phe290. On the other hand, Tyr290 can stabilize the partially protonated states of Tyr48 and Glu335 through the hydrogen-bonding network, and the polarized Tyr290 itself can be stabilized by bulk water molecules. After providing the hydrogen atom shared by Glu335 and Tyr48 to β-glucose, Glu335-COO^- and Tyr48-O^- are generated; however, the latter accepts a proton from Tyr290, and the resultant Tyr290-O^- is easily protonated by bulk water. Thus, the condensation by F290Y proceeds more quickly, due to its advantage of the hydrogen-binding network, than WT. The condensation is a valuable reaction for producing important oligosaccharides from low-cost carbohydrates. Therefore, the rapid synthesis of isomaltose from glucose using F290Y can be a new approach to generate one of the most demanded saccharides in the industry.

Although many GAMases and GDXases can cleave both α-1,4- and α-1,6-glucosidic linkages [34], IGHase has a strict specificity for α-1,6-glucosidic linkages [18]. Therefore, the atypical α-helix of IGHase is likely to be one of the key elements responsible for its high specificity for isomaltose. Here, the substitutions of Trp350 and Trp354 in this α-helix were found to decrease the k_{cat} and increase the K_m (Table 5), indicating that both residues contribute to forming subsite +1 and maintaining the catalytic residues. In addition, Trp350 is located at 3.7 Å from Trp354 (between Cζ3 and Cζ3), and Trp354 is located at 4.5 Å from Tyr48 (between Cζ3 and Cε1). Thus, Trp350 and Trp354 appear to, indirectly and directly, orient Tyr48 into the appropriate position to catalyze the reaction. In addition, the spatial position of Trp350 was found to be well-aligned with Trp582 in the *A. globiformis* GDXase (Figure 3D), which is responsible for the enzyme's high specificity for α-1,6-glucan [13]. However, here, the W350A mutant of IGHase was found to retain a high specificity for the α-1,6-glucosidic linkage (Table 6). On the other hand, W354A displayed a broad specificity and detectable hydrolysis activity toward other glucobioses. Thus, the substrate recognition mechanism of GDXases and IGHase may be different despite their similar regioselectivities.

In conclusion, we propose that Tyr48 of IGHase has a unique function among the GH15 enzymes. Tyr48 may be deprotonated independently from the other residues. The protonated form of Tyr48-OH supports the catalytic base Glu335-COO^-, and the deprotonated form of Tyr48-OH, Tyr48-O^-, can function as the second general base residue to activate a catalytic

water molecule. This property of Tyr48 appears to depend on Phe290. The atypical Phe290 causes the lack of a hydrogen-bonding network with Tyr48 and Glu335, thus contributing to the unique pH-activity profile of IGHase among the GH15 enzymes. Furthermore, we found that we could improve the condensation reaction by IGHase by modifying the hydrogen-bonding network around Tyr48. The structural insights into the condensation process will help enhance the generation of isomaltose from glucose, such as by constructing the F290Y mutant.

Materials and methods

Enzyme preparation

The plasmids (Kfla1896/pET28, Kfla1896_E178A/pET28, and Kfla1896_E335A/pET28) expressing the wild-type (WT; gene locus: *Kfla_1896*) and mutant (E178A and E335A) N-terminal His_6-tagged IGHases were constructed previously [18]. Site-directed mutagenesis was performed with PCR using the PrimeSTAR mutagenesis basal kit (Takara Bio) and the following oligonucleotide primers for Tyr48→Phe (5′-TCGGCGTTTCGGGGCTATGCCTGGCTG-3′ and 5′-GCCCCGAAACGCCGAGAAGGTCGGTGC-3′), Phe290→Tyr (5′-GACGTGTATTACGGGGGTGGGCAGTGG-3′ and 5′-CCCGTAATACACGTCCGCCGCGAACCG-3′), Trp350→Ala (5′-GCGGAGGCGGTCGCGCGCTGGGGCACG-3′ and 5′-CGCGACCGCCTCCGCGCGGGACCCGGG-3′), and Trp354→Ala (5′-GCGCGCGCGGGCACGGTGGCCACTCCG-3′ and 5′-CGTGCCCGCGCGCGACCCACTCCGC-3′), with the underlined nucleotides indicating the mutated codons.

The *E. coli* Rosetta (DE3) (Novagen) cells transformed with each plasmid were grown in Luria-Bertani medium containing 50 mg/L kanamycin at 37°C. When the A_{600} reached 0.5–0.7, the culture broth was cooled on ice for 30 min, and protein expression was induced by adding 0.1 mM isopropyl β-D-thiogalactopyranoside and allowing the cells to incubate at 20°C for 6 h.

The cells were harvested by centrifugation (10,000 x *g* at 4°C for 5 min), resuspended in Buffer-A (20 mM sodium phosphate buffer, pH 7.0 and 0.3 M NaCl), and disrupted by sonication. The cell-free lysate obtained by centrifugation (6,000 x *g* at 4°C for 20 min) was applied to a Ni-chelating Sepharose Fast Flow column (Cytiva). After the column was washed with 20 mM imidazole in Buffer-A, the adsorbed proteins were eluted with a 20–500 mM imidazole linear gradient in Buffer-A. The active fractions were dialyzed against Buffer-B (20 mM sodium phosphate buffer, pH 8.0) and loaded onto a DEAE-Sepharose Fast Flow column (Cytiva). The column was washed with Buffer-B, and the absorbed proteins were eluted with a

linear gradient of 0–1 M NaCl in Buffer-B. The electrophoretically homogenous fractions were dialyzed against 20 mM HEPES buffer (pH 8.0) and concentrated using Vivaspin20 (30kDa) (Sartorius). The concentrations of the purified enzymes were determined by measuring their absorbance at 280 nm using the ProtParam-calculated extinction coefficient [35]: WT, 112,410; Y48F, 110,920; E178A, 112,410; F290Y, 108,400; E335A, 112,410; W350A, 106,910; W354A, 106,910.

Crystallization, data collection, and processing

All crystallizations were performed using the hanging drop vapor diffusion method at 20°C for approximately 1 week. PEGRx 1/2 and SalRx 1/2 (Hampton Research) were used for the first crystallization screen. Several crystals were obtained in a drop composed of 3 μL of each protein at approximately 20 mg/mL and 3 μL of reservoir solution [100 mM sodium citrate buffer (pH 5.5), 200 mM ammonium citrate tribasic (pH 6.8), and 10–15% polyethylene glycol monomethyl ether 2,000 (PEG-ME2K) with the final pH of 6.1]. Each well of a 48-well plate for crystallization contained 200 μL of solution having the same composition as the reservoir solution. Co-crystallization of E335A with isomaltose was performed by adding 1 μL of 10 mM isomaltose (Tokyo Chemical Industry) into the drop when we set up it. For the structure analysis of WT and F290Y at pH 4.5 and pH 8.0, they were crystallized in drops composed of 3 μL of each protein and 3 μL of reservoir solution [200 mM ammonium citrate tribasic (pH 7.0 or 8.0) and 8% PEG-ME2K], and their pH were changed to pH 4.5 or 8.0 with a cryoprotectant as mentioned below.

The data set for native SAD was collected using the solution-free mount method [36] from a single crystal of E335A at beamline BL17A of the Photon Factory (Tsukuba, Japan) at a wavelength of 2.1 Å. The high-resolution data sets were collected at beamlines BL38B1 of SPring-8 (Hyogo, Japan) and NE3A and AR-NW12A of the Photon Factory at a wavelength of 1.0 Å. Each crystal was flash cooled after soaking in a reservoir solution containing 20% glycerol; 2 mM isomaltose was added for the co-crystals. In the case of structural analysis of WT and F290Y at pH 4.5, each crystal formed at pH 7.0 was soaked into a cryoprotectant composed of 200 mM ammonium citrate tribasic (pH 4.5), 8% PEG-ME2K, and 20% glycerol. All the crystals were exposed to the X-ray beam under a stream of nitrogen at 100 K, and diffraction data sets were indexed, integrated, scaled, and merged with XDS [37]. The phase problem for IGHase was solved by native SAD. Seven out of nine sulfur sites were found (occ > 0.6) by SHELX [38] and HKL2MAP [39]. Phasing, density modification, and preliminary model building were performed using PHENIX AutoSol [40]. Out of the 405 amino acids in one molecule, 341 were successfully built and used as the initial model for the following procedure. The data collection statistics of native SAD is shown in Table 3. The high-resolution structures were determined by the molecular replacement method with AutoMR in PHENIX

[41] using the initial model as a search model. Manual model corrections and anisotropic refinements, except for the isotropic refinement of E178A, WT (pH 4.5), and F290Y (pH 4.5 and 8.0), were performed using Coot [42], REFMAC5 [43] in CCP4, and phenix.refine [44] in PHENIX. The coordinates and structure factors have been deposited in the Protein Data Bank with accession numbers 5Z3A (WT at pH 6.1), 5Z3B (Y48F), 5Z3C (E178A), 5Z3D (F290Y at pH 6.1), 5Z3E (E335A), 5Z3F (E335A bound to glucose), 7C24 (F290Y at pH 8.0), 7C25 (WT at pH 8.0), 7C26 (WT at pH 4.5), and 7C27 (F290Y at pH 4.5). The data collection and refinement statistics were summarized in Table 4 and 7. The graphical representations in this report were prepared using the PyMOL Molecular Graphics System Version 2.0 (Schrödinger, LLC). Polder map was generated with phenix.polder [45].

Docking simulations

The coordinates of isomaltose were extracted from a PDB file (PDB ID: 5AWP) and used as the ligand. The PDBQT files of the ligand and the enzyme [WT at pH 6.1 and Y48F in which Tyr(Phe)48, Arg113, Glu178, Glu179 and Glu335 were treated as flexible] were prepared using AutoDockTools [46], and the docking experiments were performed using AutoDock Vina [47].

Kinetic analysis

Enzyme activity was measured at 35°C in a standard reaction mixture containing 40 mM sodium acetate buffer (pH 6.0), 2 mM isomaltose, and an enzyme diluted to an appropriate concentration using 20 mM HEPES buffer (pH 8.0) containing 0.1% Triton X-100. The reaction was stopped at 10 min by the addition of two times the volume of 2 M Tris-HCl (pH 7.0) to the reaction mixture. Then, the glucose concentration was measured using a GlucoseCII-test Wako kit (Fujifilm Wako Pure Chemical). One unit was defined as the amount of enzyme that hydrolyzed 1 μmol of isomaltose per min under the standard conditions.

Substrate specificity was analyzed by measuring the initial velocities of the hydrolysis of various substrates at 10 mM under the standard conditions except when using Britton-Robinson buffer (pH 5.5) as the reaction buffer.

The initial velocities for the hydrolysis of isomaltose (0.67–4.0 mM) in Britton-Robinson buffer (pH 4.2–8.4) were measured under the standard conditions. The kinetic parameters, k_{cat} and K_m, were determined from the s vs. $v/[E]_0$ plots by fitting to the Michaelis-Menten equation using KaleidaGraph 3.6J (Synergy Software). The mean with standard deviation of triplicate measurements is summarized in Table 1. As the K_m value at pH 4.2 was too high to be determined from the s vs. $v/[E]_0$ plots, only the k_{cat}/K_m value was estimated from the $1/s$ vs. $[E]_0/v$ plots. The values of the constants (k_1, k_2, K_{s2}, k/K_{s2}, k_2/K_{s3}), pK_{es1}–pK_{es3}, and pK_{e1}–pK_{e3} were determined from the pH vs. k_{cat} plots and pH vs. k_{cat}/K_m plots by fitting to Eqs. 1 and 2 describing Scheme 1 or to Eqs. 3 and 4 describing Scheme 2 (Figure 1B).

Eq. 1) $k_{\mathrm{cat}} = \frac{k_1}{1+10^{\mathrm{p}K_{\mathrm{es1}}-\mathrm{pH}}+10^{\mathrm{pH}-\mathrm{p}K_{\mathrm{es2}}}}$

Eq. 2) $\frac{k_{\mathrm{cat}}}{K_{\mathrm{m}}} = \frac{k_1/K_{\mathrm{s2}}}{1+10^{\mathrm{p}K_{\mathrm{e1}}-\mathrm{pH}}+10^{\mathrm{pH}-\mathrm{p}K_{\mathrm{e2}}}}$

Eq. 3) $k_{\mathrm{cat}} = \frac{k_1+k_2\cdot 10^{\mathrm{pH}-\mathrm{p}K_{\mathrm{es2}}}}{1+10^{\mathrm{p}K_{\mathrm{es1}}-\mathrm{pH}}+10^{\mathrm{pH}-\mathrm{p}K_{\mathrm{es2}}}+10^{2\mathrm{pH}-\mathrm{p}K_{\mathrm{es2}}-\mathrm{p}K_{\mathrm{es3}}}}$

Eq. 4) $\frac{k_{\mathrm{cat}}}{K_{\mathrm{m}}} = \frac{{k_1}/{K_{\mathrm{s2}}}+{k_2}/{K_{\mathrm{s3}}}\cdot 10^{\mathrm{pH}-\mathrm{p}K_{\mathrm{e2}}}}{1+10^{\mathrm{p}K_{\mathrm{e1}}-\mathrm{pH}}+10^{\mathrm{pH}-\mathrm{p}K_{\mathrm{e2}}}+10^{2\mathrm{pH}-\mathrm{p}K_{\mathrm{e2}}-\mathrm{p}K_{\mathrm{e3}}}}$

Condensation with glucose

The WT, Y48F, or F290Y enzyme at 5 μM was incubated with 1 M glucose in 40 mM sodium acetate buffer (pH 5.5) at 30°C, and an aliquot of the mixture was incubated at 100°C for 1 min to stop the reaction.

The products were preliminarily analyzed by TLC (Silica Gel 60 aluminum plate; Merck Millipore) using a developing solvent of acetonitrile/H_2O (80/20, v/v), followed by the visualization treatment with a reagent containing 0.03% 1-naphthol and 5% sulfuric acid in methanol and heating. The concentration of isomaltose was determined using a high-performance anion-exchange chromatography system equipped with a pulsed amperometric detector and CarboPac PA1 column (Φ 4 x 250 mm; Thermo Fischer Scientific). The sugars were eluted with an isocratic mobile phase of 80 mM NaOH at a flow rate of 0.8 ml/min. Isomaltose (10–300 μM) and sorbitol (100 μM) were used as the standard and internal standard, respectively.

Author contributions

TT conceived the study. TT, MO, and Atsuo K designed the study. TT, MC, and YT crystallized the enzymes and determined their crystal structures. TT, YF, Asako K, MO, and TI performed expression, purification, and kinetic analysis of the enzymes. YF, JS and WL analyzed the condensation products. TT, MO, YT, MY, and Atsuo K discussed the data. TT and MC wrote a draft, and MO, YT, MY and Atsuo K revised the draft. All authors reviewed the manuscript.

Acknowledgments

We thank the staff of beamlines BL38B1 at SPring-8 (experimental proposal number 2017B2725) and NE3A, BL17A, and AR-NW12A at the Photon Factory for help with the data collection. This research is partially supported by the Platform Project for Supporting

Drug Discovery and Life Science Research (Basis for Supporting Innovative Drug Discovery and Life Science Research (BINDS)) from the Japan Agency for Medical Research and Development (AMED) under Grant Number JP18am0101071. We also thank Dr. K. Kihira at Japan Aerospace Exploration Agency (JAXA) for helping us with the optimization of crystallization conditions. In addition, this work was partly supported in part by the Japan Society for the Promotion of Science KAKENHI Grant Nos. 17H03801, 18K19159, and 19K16064.

References

1 Yamamoto T (1994) *Enzyme chemistry and molecular biology of amylases and related enzymes* CRC Press, Boca Raton.

2 Ruddock LW & Molinari M (2006) N-glycan processing in ER quality control. *J Cell Sci* **119**, 4373–4380.

3 Okuyama M, Miyamoto M, Matsuo I, Iwamoto S, Serizawa R, Tanuma M, Ma M, Klahan P, Kumagai Y, Tagami T & Kimura A (2017) Substrate recognition of the catalytic α-subunit of glucosidase II from *Schizosaccharomyces pombe*. *Biosci Biotechnol Biochem* **81**, 1503–1511.

4 Garvey M, Klose H, Fischer R, Lambertz C & Commandeur U (2013) Cellulases for biomass degradation: Comparing recombinant cellulase expression platforms. *Trends Biotechnol* **31**, 581–593.

5 Ngiwsara L, Iwai G, Tagami T, Sato N, Nakai H, Okuyama M, Mori H & Kimura A (2011) Amino acids in conserved region II are crucial to substrate specificity, reaction velocity, and regioselectivity in the transglucosylation of honeybee GH-13 α-glucosidases. *Biosci Biotechnol Biochem* **76**, 1967–1974.

6 Ma M, Okuyama M, Sato M, Tagami T, Klahan P, Kumagai Y, Mori H & Kimura A (2017) Effects of mutation of Asn694 in *Aspergillus niger* α-glucosidase on hydrolysis and transglucosylation. *Appl Microbiol Biotechnol* **101**, 6399–6408.

7 Ma M, Okuyama M, Tagami T, Kikuchi A, Klahan P & Kimura A (2019) Novel α-1,3/α-1,4-glucosidase from *Aspergillus niger* exhibits unique transglucosylation to generate high levels of nigerose and kojibiose. *J Agric Food Chem* **67**, 3380–3388.

8 Song K-M, Okuyama M, Nishimura M, Tagami T, Mori H & Kimura A (2013) Aromatic residue on β→α loop 1 in the catalytic domain is important to the transglycosylation specificity of glycoside hydrolase family 31 α-glucosidase. *Biosci Biotechnol Biochem* **77**, 1759–1765.

9 Tagami T, Tanaka Y, Mori H, Okuyama M & Kimura A (2013) Enzymatic synthesis of acarviosyl-maltooligosaccharides using disproportionating enzyme 1. *Biosci Biotechnol Biochem* **77**, 312–319.

10 Okuyama M, Matsunaga K, Watanabe KI, Yamashita K, Tagami T, Kikuchi A, Ma M, Klahan P, Mori H, Yao M & Kimura A (2017) Efficient synthesis of α-galactosyl oligosaccharides using a mutant *Bacteroides thetaiotaomicron* retaining α-galactosidase (BtGH97b). *FEBS J* **284**, 766–783.

11 Lombard V, Golaconda Ramulu H, Drula E, Coutinho PM & Henrissat B (2013) The carbohydrate-active enzymes database (CAZy) in 2013. *Nucleic Acids Res* **42**, D490–D495.

12 Henrissat B (1991) A classification of glycosyl hydrolases based on amino acid sequence similarities. *Biochem J* **280**, 309–316.

13 Mizuno M, Tonozuka T, Suzuki S, Uotsu-Tomita R, Kamitori S, Nishikawa A & Sakano Y (2004) Structural insights into substrate specificity and function of glucodextranase. *J Biol Chem* **279**, 10575–10583.

14 Carroll JD, Pastuszak I, Edavana VK, Pan YT & Elbein AD (2007) A novel trehalase from *Mycobacterium smegmatis* - Purification, properties, requirements. *FEBS J* **274**, 1701–1714.

15 Sakaguchi M, Shimodaira S, Ishida S, Amemiya M, Honda S, Sugahara Y, Oyama F & Kawakita M (2015) Identification of GH15 family thermophilic archaeal trehalases that function within a narrow acidic-pH range. *Appl Environ Microbiol* **81**, 4920–4931.

16 Sadahiro J, Mori H, Saburi W, Okuyama M & Kimura A (2015) Extracellular and cell-associated forms of *Gluconobacter oxydans* dextran dextrinase change their localization depending on the cell growth. *Biochem Biophys Res Commun* **456**, 500–505.

17 Jeong WS, Kim YR, Hong SJ, Choi SJ, Choi JH, Park SY, Woo EJ, Kim YM & Park BR (2019) Carboxy-terminal region of a thermostable citase from *Thermoanaerobacter thermocopriae* has the ability to produce long isomaltooligosaccharides. *J Microbiol Biotechnol* **29**, 1938–1946.

18 Tagami T, Miyano E, Sadahiro J, Okuyama M, Iwasaki T & Kimura A (2016) Two novel glycoside hydrolases responsible for the catabolism of cyclobis-(1→6)-α-nigerosyl. *J Biol Chem* **291**, 16438–16447.

19 Hiromi K, Takahashi K, Hamauzu Z & Ono S (1966) Kinetic studies on gluc-amylase: III. The influence of pH on the rates of hydrolysis of maltose and panose. *J Biochem* **59**, 469–475.

20 Hiromi K, Kawai M & Ono S (1966) Kinetic studies on gluc-amylase: IV. hydrolysis of isomaltose. *J Biochem* **59**, 476–480.

21 Svensson B, Clarke AJ, Svendesen I & Møller H (1990) Identification of carboxylic acid residues in glucoamylase G2 from *Aspergillus niger* that participate in catalysis and substrate binding. *Eur J Biochem* **188**, 29–38.

22 Aleshin A, Golubevs A, Firsov LM & Honzatko RB (1992) Crystal Structure of Glucoamylase from *Aspergillus awamori* var. X100 to 2.2-A Resolution. *J Biol Chem* **267**, 19291–19298.

23 Harris EMS, Aleshin AE, Firsov LM & Honzatko RB (1993) Refined structure for the complex of 1-deoxynojirimycin with glucoamylase from *Aspergillus awamori* var. X100 to 2.4-Å resolution. *Biochemistry* **32**, 1618–1626.

24 Aleshin AE, Hoffman C, Firsov LM & Honzatko RB (1994) Refined crystal structures of glucoamylase from *Aspergillus awamori* var. X100. *J Mol Biol* **238**, 575–591.

25 McCarter JD & Withers SG (1994) Mechanisms of enzymatic glycoside hydrolysis. *Curr Opin Struct Biol* **4**, 885–892.

26 Brocklehurst K & Dixon HBF (1976) pH-dependence of the steady-state rate of a two-step enzymic reaction. *Biochem J* **155**, 61–70.

27 Holm L & Laakso LM (2016) Dali server update. *Nucleic Acids Res* **44**, W351–W355.

28 Davies GJ, Wilson KS & Henrissat B (1997) Nomenclature for sugar-binding subsites in glycosyl hydrolases. *Biochem J* **321**, 557–559.

29 Coutinho PM & Reilly PJ (1994) Structure-function relationships in the catalytic and starch binding domains of glucoamylase. *Protein Eng Des Sel* **7**, 393–400.

30 McIntosh LP, Hand G, Johnson PE, Joshi MD, Körner M, Plesniak L, Ziser L, Wakarchuk WW & Withers SG (1996) The pKa of the general acid/base carboxyl group of a glycosidase cycles during catalysis: A ^{13}C-NMR study of Bacillus circulans xylanase. *Biochemistry* **35**, 9958–9966.

31 Watts AG, Damager I, Amaya ML, Buschiazzo A, Alzari P, Frasch AC & Withers SG (2003) *Trypanosoma cruzi* trans-sialidase operates through a covalent sialyl−enzyme intermediate: Tyrosine is the catalytic nucleophile. *J Am Chem Soc* **125**, 7532–7533.

32 Frandsen TP, Dupont C, Lehmbeck J, Staffer B, Sierks MR, Honzatko RB & Svensson B (1994) Site-directed mutagenesis of the catalytic base glutamic acid 400 in glucoamylase from *Aspergillus niger* and of tyrosine 48 and glutamine 401, goth hydrogen-bonded to the γ-carboxylate group of glutamic acid 400. *Biochemistry* **33**, 13808–13816.

33 Nerinckx W, Desmet T, Piens K & Claeyssens M (2005) An elaboration on the syn-anti proton donor concept of glycoside hydrolases: Electrostatic stabilisation of the transition state as a general strategy. *FEBS Lett* **579**, 302–312.

34 Uotsu-Tomita R, Tonozuka T, Sakai H & Sakano Y (2001) Novel glucoamylase-type enzymes from *Thermoactinomyces vulgaris* and *Methanococcus jannaschii* whose genes

are found in the flanking region of the α-amylase genes. *Appl Microbiol Biotechnol* **56**, 465–473.

35 Gasteiger E, Hoogland C, Gattiker A, Duvaud S, Wilkins MR, Appel RD & Bairoch A (2005) Protein identification and analysis tools on the ExPASy server. In *The Proteomics Protocols Handbook* (Walker JM, ed), 1st ed., pp. 571–607. Humana Press.

36 Kitago Y, Watanabe N & Tanaka I (2005) Structure determination of a novel protein by sulfur SAD using chromium radiation in combination with a new crystal-mounting method. *Acta Crystallogr Sect D Biol Crystallogr* **61**, 1013–1021.

37 Kabsch W (2010) XDS. *Acta Crystallogr Sect D Biol Crystallogr* **66**, 125–132.

38 Sheldrick GM (2008) A short history of SHELX. *Acta Crystallogr Sect A Found Crystallogr* **64**, 112–122.

39 Pape T & Schneider TR (2004) HKL2MAP : A graphical user interface for macromolecular phasing with SHELX programs. *J Appl Crystallogr* **37**, 843–844.

40 Terwilliger TC, Adams PD, Read RJ, McCoy AJ, Moriarty NW, Grosse-Kunstleve RW, Afonine P V, Zwart PH & Hung LW (2009) Decision-making in structure solution using Bayesian estimates of map quality: The PHENIX AutoSol wizard. *Acta Crystallogr Sect D Biol Crystallogr* **65**, 582–601.

41 Adams PD, Afonine P V, Bunkóczi G, Chen VB, Davis IW, Echols N, Headd JJ, Hung LW, Kapral GJ, Grosse-Kunstleve RW, McCoy AJ, Moriarty NW, Oeffner R, Read RJ, Richardson DC, Richardson JS, Terwilliger TC & Zwart PH (2010) PHENIX: A comprehensive Python-based system for macromolecular structure solution. *Acta Crystallogr Sect D Biol Crystallogr* **66**, 213–221.

42 Emsley P, Lohkamp B, Scott WG & Cowtan K (2010) Features and development of Coot. *Acta Crystallogr Sect D Biol Crystallogr* **66**, 486–501.

43 Vagin AA, Steiner RA, Lebedev AA, Potterton L, McNicholas S, Long F & Murshudov GN (2004) REFMAC5 dictionary: Organization of prior chemical knowledge and guidelines for its use. *Acta Crystallogr Sect D Biol Crystallogr* **60**, 2184–2195.

44 Afonine P V., Grosse-Kunstleve RW, Echols N, Headd JJ, Moriarty NW, Mustyakimov M, Terwilliger TC, Urzhumtsev A, Zwart PH & Adams PD (2012) Towards automated crystallographic structure refinement with phenix.refine. *Acta Crystallogr Sect D Biol Crystallogr* **68**, 352–367.

45 Liebschner D, Afonine P V., Moriarty NW, Poon BK, Sobolev O V., Terwilliger TC & Adams PD (2017) Polder maps: Improving OMIT maps by excluding bulk solvent. *Acta Crystallogr Sect D Struct Biol* **73**, 148–157.

46 Morris GM, Huey R, Lindstrom W, Sanner MF, Belew RK, Goodsell DS & Olson AJ (2009) AutoDock4 and AutoDockTools4: Automated docking with selective receptor flexibility. *J Comput Chem* **30**, 2785–2791.

47 Trott O & Olson AJ (2010) AutoDock Vina: Improving the speed and accuracy of docking with a new scoring function, efficient optimization, and multithreading. *J Comput Chem* **31**, 455–461.

48 Kawabata T (2003) MATRAS: A program for protein 3D structure comparison. *Nucleic Acids Res* **31**, 3367–3369.

49 Robert X & Gouet P (2014) Deciphering key features in protein structures with the new ENDscript server. *Nucleic Acids Res* **42**, W320–W324.

Table 1. Kinetic parameters of WT and F290Y for hydrolysis of isomaltose at various pH

	WT			F290Y		
pH	k_{cat} (s^{-1})	K_m (mM)	k_{cat}/K_m (s^{-1} mM^{-1})	k_{cat} (s^{-1})	K_m (mM)	k_{cat}/K_m (s^{-1} mM^{-1})
4.2	n.d.[a)]	n.d. [a)]	0.687 ±0.017	n.d. [a)]	n.d. [a)]	0.441 ±0.011
4.6	14.4 ±0.2	2.02 ±0.08	7.16	11.9 ±0.0	1.48 ±0.05	8.05
5.0	16.3 ±0.2	1.20 ±0.02	13.6	12.8 ±0.1	1.09 ±0.04	11.8
5.5	17.7 ±0.1	1.03 ±0.01	17.1	15.6 ±0.2	1.02 ±0.04	15.3
6.2	22.0 ±0.1	1.09 ±0.01	20.1	17.2 ±0.0	0.974 ±0.013	17.7
6.5	23.4 ±0.3	1.41 ±0.03	16.6	16.0 ±0.5	1.07 ±0.08	14.9
7.2	20.4 ±0.3	1.84 ±0.06	11.1	12.6 ±0.0	1.09 ±0.04	11.6
7.9	10.8 ±0.2	1.60 ±0.09	6.78	5.77 ±0.04	1.37 ±0.07	4.21
8.4	2.16 ±0.05	0.615 ±0.057	3.53	1.69 ±0.04	1.29 ±0.09	1.31

a) Not determined

Table 2. The regression analysis of pH profiles of the WT and F290Y IGHase

Scheme 1

	pH vs. k_{cat} plots				pH vs. k_{cat}/K_m plots				
Enzyme	k_1 (s^{-1})	pK_{es1}	pK_{es2}	R^2	k_1 (s^{-1})	K_{s2} (mM)	pK_{e1}	pK_{e2}	R^2
WT	23	4.5	7.8	0.922	20	0.98	4.9	7.4	0.927
F290Y	17	4.3	7.6	0.978	21	1.1	4.8	7.4	0.958

Scheme 2

	pH vs. k_{cat} plots						pH vs. k_{cat}/K_m plots					
Enzyme	k_1 (s^{-1})	k_2 (s^{-1})	pK_{es1}	pK_{es2}	pK_{es3}	R^2	k_1/K_{s2} (s^{-1} mM^{-1})	k_2/K_{s3} (s^{-1} mM^{-1})	pK_{e1}	pK_{e2}	pK_{e3}	R^2
WT	16	29	3.7	6.2	7.6	0.988	25	8.5	5.0	6.6	8.3	0.970
F290Y	13	18	3.7	5.6	7.5	0.988	0.21	18	4.6	4.5	7.4	0.976

R^2, Determination coefficient of the regression

Table 3. Data collection statistics of native SAD

Enzyme	E335A
Diffraction source	PF BL17A
Data processing	
Space group	$P42_12$
Unit-cell parameters (Å)	105.31, 105.31, 89.58
Resolution range (Å)	50–2.5 (2.65–2.5)
Total No. of reflections	4298527
No. of unique reflections	33236
Completeness (%)	99.8 (98.2)
Multiplicity	129.33 (87.75)
Average I/σ (I)	60.8 (16.4)
R_{mean} (%)	12.0 (45.1)
R_{sym} (%)	12.0 (44.8)
$CC_{1/2}$	100 (98.6)
SigAno	1.335

The parenthesized values are for the highest-resolution shell.

Table 4. Data collection and refinement statistics of the X-ray crystal structure analysis

Enzyme	WT	Y48F	E178A	F290Y	E335A	E335A_Glc
PDBID	5Z3A	5Z3B	5Z3C	5Z3D	5Z3E	5Z3F
Diffraction source	SP8 BL38B1	SP8 BL38B1	PF NE3A	SP8 BL38B1	PF NE3A	PF NE3A
Data processing						
Space group	$P42_12$	$P42_12$	$P42_12$	$P42_12$	$P42_12$	$P42_12$
Unit-cell parameters (Å)	104.74, 104.74, 89.49	104.66, 104.66, 89.38	104.92, 104.92, 89.50	104.73, 104.73, 89.32	104.81, 104.81, 89.46	104.83, 104.83, 89.45
Mosaicity (°)	0.107	0.094	0.228	0.110	0.067	0.065
Resolution range (Å)	46.84-1.40 (1.48-1.40)	45.16-1.25 (1.33-1.25)	45.26-1.60 (1.69-1.60)	45.17-1.25 (1.31-1.25)	45.22-1.10 (1.16-1.10)	46.88-1.10 (1.16-1.10)
Total No. of reflections	1411079 (223322)	1959309 (305423)	1437029 (66196)	1966471 (136955)	3764592 (199948)	3771335 (200183)
No. of unique reglections	97738 (15544)	136595 (21801)	225797 (10506)	309010 (21831)	495774 (31816)	497311 (31945)
Completeness (%)	99.9 (99.7)	99.9 (99.8)	99.9 (99.5)	99.8 (99.5)	99.9 (99.3)	99.9 (99.6)
Multipicity	14.4 (14.4)	14.3 (14.0)	6.4 (6.3)	6.4 (6.3)	7.6 (6.3)	18.8 (15.6)
Average I/σ(I)	26.7 (4.1)	28.0 (5.0)	38.1 (8.2)	25.8 (4.4)	23.4 (8.0)	7.6 (6.3)
Rmean(%)	6.2 (71.2)	5.6 (57.3)	6.3 (45.6)	6.0 (65.7)	8.9 (38.4)	11.5 (53.6)
Rsym(%)	5.9 (68.7)	5.4 (55.3)	6.1 (44.5)	5.7 (63.3)	8.7 (37.2)	11.2 (51.9)
CC1/2	100 (92.0)	100 (94.3)	100 (97.4)	99.9 (92.4)	99.8 (96.9)	99.7 (94.6)
Refinement						
Rwork (%)	11.58	11.13	13.38	11.33	10.76	10.76
Rfree (%)	13.97	12.51	15.71	13.40	11.84	12.09
No. atoms						
Non-solvent	2985	3005	2936	2977	2995	2983
Solvent	340	368	339	432	486	430
Hydrogen	2853	2895	2814	2858	2887	2872
Ligand	2xGOL (S-1; S+1)	1xGOL (S-1)	1xGOL (S-1)	1xGOL (S-1)	1xGOL (S-1)	1xGLC (S-1) 1xGOL (S+1)
RMSD values from ideal						
Bond (Å)	0.010	0.018	0.013	0.020	0.016	0.018
Angle (°)	1.288	1.668	1.425	1.813	1.710	1.695
Ramachandran						
Outliers (%)	0	0	0	0	0	0
Allowd (%)	2.38	2.09	2.67	1.85	2.36	1.58
Favored (%)	97.62	97.91	97.33	98.15	97.64	98.42
Clashscore	1.71	1.36	0.52	2.94	2.73	4.29

The parenthesized values are for the highest-resolution shell.
RMSD, root mean square deviation; GOL, glycerol; GLC, β-glucose; S−1, subsite −1; S+1, subsite +1

Table 5. Specific activities and kinetic parameters for isomaltose hydrolysis at pH 6.2

Enzyme	Specific activity (U/mg)	k_{cat} (s^{-1})	K_m (mM)	k_{cat}/K_m (s^{-1} mM^{-1})
WT	19.6	22.0 ± 0.1	1.09 ± 0.01	20.1
F290Y	15.8	17.2 ± 0.0	0.974 ± 0.013	17.7
W350A	0.165	0.866 ± 0.003	5.84 ± 0.16	0.149
W354A	0.161	0.461 ± 0.010	3.64 ± 0.10	0.127
Y48F	0.00566	n.d.[a)]	n.d.[a)]	n.d.[a)]
E178A	0.00161[b)]	n.d.[a)]	n.d.[a)]	n.d.[a)]
E335A	< 0.0001[b)]	n.d.[a)]	n.d.[a)]	n.d.[a)]

a) Not determined due to their low activities
b) Previously reported [18]

Table 6. Hydrolytic velocities of IGHase and its variants

Substrate (10 mM)	Velocity (μmol/min/mg) WT	F290Y	W350A	W354A
Isomaltose	28	20	0.76	0.46
Panose	3.2	1.2	0.042	0.080
Isomaltotriose	1.6	0.56	0.043	0.053
Maltose	n.d	n.d.	n.d.	0.0034
Kojibiose	0.022	0.021	n.d.	0.0039
Nigerose	n.d	n.d.	n.d.	0.0027
Trehalose	n.d	n.d.	0.0011	0.0018

n.d., Not determined due to a value of less than 8.1×10^{-4} μmol/min/mg.

Table 7. Data collection and refinement statistics of the X-ray crystal structure analysis of WT and F290Y at various pH

Enzyme	WT_pH4.5	WT_pH8.0	F290Y_pH4.5	F290Y_pH8.0
PDB ID	7C26	7C25	7C27	7C24
Diffraction source	PF AR-NW12A	PF AR-NW12A	PF AR-NW12A	PF AR-NW12A
Data processing				
Space group	$P42_12$	$P42_12$	$P42_12$	$P42_12$
Unit-cell parameters (Å)	105.35, 105.35, 90.33	105.46, 105.46, 89.95	104.81, 104.81, 90.16	104.81, 104.81, 89.82
Mosaicity (°)	0.229	0.156	0.290	0.320
Resolution range (Å)	47.16-1.80 (1.91-1.80)	47.21-1.50 (1.60-1.50)	46.92-1.91 (2.02-1.91)	41.59-1.71 (1.81-1.71)
Total No. of reflections	1064405 (160303)	1948073 (310198)	1050688 (168237)	1429234 (222715)
No. of unique reflections	41276 (6071)	74640 (12800)	39724 (6298)	54864 (8723)
Completeness (%)	87.1 (80.6)	92.6 (99.7)	99.9 (99.8)	99.9 (99.7)
Multiplicity	25.8 (26.4)	26.1 (24.2)	26.4 (26.7)	26.1 (25.5)
Average I/σ(I)	28.6 (2.3)	26.5 (2.8)	10.7 (1.0)	13.4 (0.84)
R_{mean}(%)	8.2 (161.7)	7.7 (135.7)	24.2 (372.2)	22.6 (466.7)
R_{sym}(%)	8.0 (158.6)	7.6 (132.9)	23.8 (365.1)	22.2 (457.5)
$CC_{1/2}$	99.9 (90.6)	100 (85.5)	99.8 (42.9)	99.9 (52.9)
Refinement				
R_{work} (%)	17.58	13.61	18.19	16.33
R_{free} (%)	20.61	17.26	21.17	18.94
No. atoms				
Non-solvent	2985	3005	2936	2977
Solvent	340	368	339	432
Hydrogen	2853	2895	2814	2858
Ligand	2XGOL (S-1; S+1)	2XGOL (S-1; S+1)	2XGOL (S-1; S+1)	2XGOL (S-1; S+1)
RMSD values from ideal				
Bond (Å)	0.010	0.018	0.013	0.020
Angle (°)	1.288	1.668	1.425	1.813
Ramachandran				
Outliers (%)	0	0	0	0
Allowed (%)	2.38	2.09	2.67	1.85
Favored (%)	97.62	97.91	97.33	98.15
Clashscore	1.71	1.36	0.52	2.94

The parenthesized values are for the highest-resolution shell.
RMSD, root mean square deviation; GOL, glycerol; S−1, subsite −1; S+1, subsite +1

Figure legends

Figure 1. pH-hydrolysis profile of IGHase

(A) pH vs. k_{cat} plots and pH vs. k_{cat}/K_m plots of WT (upper two panels) and F290Y (lower two panels). The regression curves derived from schemes 1 and 2 (Figure lB) are drawn in dotted and solid lines, respectively. Each k_{cat} and k_{cat}/K_m value were represented as mean ± SD of triplicated measurement. (B) The reaction schemes of the traditional two-residue-dependent process (Scheme 1) and a three-residue-dependent process (Scheme 2).

Figure 2. Overall structure of IGHase

(A) The overall structure of wild-type IGHase. The color spectrum is shown as blue (N terminus) to red (C terminus). Two glycerol molecules in the active pocket are drawn as sticks. The arrow indicates the extra α-helix. The model was drawn by PyMOL. (B) Topology models of the catalytic domains of GH15 enzymes. Circle and triangle represent α-helix and β-strand, respectively. The numerals are the sequence of the α-helices forming $(\alpha/\alpha)_6$-barrel fold. The red circle indicates the extra atypical α-helix insertion observed solely in isomaltose glucohydrolase (left upper panel; PDB ID: 5Z3A). Right upper panel, glucodextranase from *Arthrobacter globiformis* (PDB ID: 1ULV); Left lower panel, glucoamylase from *Thermoanaerobacterium thermosaccharolyticum* (PDB ID: 1LF9); Right lower panel, glucoamylase from *Aspergillus awamori* (PDB ID: 1GAI).

Figure 3. Substrate recognition of IGHase

(A) The active site structure of E335A co-crystallized with isomaltose (E335A_Glc). The electron densities observed in the active pocket fit well to a β-glucose and a glycerol. The contour level of the polder map is 5σ. The residue color is the same as Figure 2A. The yellow dashed lines indicate hydrogen bonds, and −1 and +1 represent the subsite positions. (B) Superimposition of the docking model of WT with isomaltose (blue) and E335A_Glc (green). (C) Multiple sequence alignment of GH15 enzymes produced using MATRAS [48] and depicted using ESPript 3.0 server (http://espript.ibcp.fr) [49]. The active site residues (asterisks) and catalytic residues (black triangles) are indicated. AgGD, *Arthrobacter globiformis* GDXase; TtGA, *Thermoanaerobacterium thermosaccharolyticum* GAMase; AaGA, *Aspergillus awamori* GAMase; AnGA_3EQA, *Aspergillus niger* CBS 513.88 GAMase; AnGA_6FRV, *As. niger* TCCC41661 GAMase; ArGA, *Amorphotheca resinae* GAMase; PoGA, *Penicillium oxalicum* GAMase; TrGA, *Trichoderma reesei* GAMase; SfGA, *Saccharomycopsis fibuligera* GAMase. (D) The superimposition of IGHase E335A_Glc (green; glucose and glycerol are drawn as stick models), GDXase from *Ar.*

globiformis (cyan; PDB ID: 1ULV), GAMase from *T. thermosaccharolyticum* (magenta; PDB ID: 1LF9), and GAMase from *As. awamori* (yellow; PDB ID: 1GAI). The residue numbers of IGHase are denoted. All models were drawn by PyMOL.

Figure 4. Hydrogen-bonding network around Tyr48

Superimpositions of WT (green) on F290Y (A; yellow), Y48F (B; cyan), E335A (C; pink) or E335A_Glc (D; purple). The black dashed lines indicate the hydrogen-bonding network of Tyr290–Tyr48–Glu335 in F290Y. All models were drawn by PyMOL.

Figure 5. Docking models of WT and Y48F

Superimposition of the docking models of WT with isomaltose (green) and Y48F with isomaltose (magenta). They were aligned using the align command in PyMOL with the ligand molecules (stick models) and the hydrogen bonds (yellow dashed lines).

Figure 6. Condensation catalyzed by IGHase and its mutants

(A) TLC analysis of the reaction mixtures of 5 μM WT, Y48F, or F290Y at 5 and 23 h. Lanes Std.: glucose (Glc), isomaltose (IG2), and panose (Pan). (B) Time course of isomaltose synthesis by the condensation of WT (black) and F290Y (red). The data were represented as mean ± SD.

Figure 7. Crystal structures of IGHase (WT and F290Y) at various pH

Overall (A) and active-site (B) structures of WT at pH 4.5 (magenta), pH 6.1 (green), and pH 8.0 (yellow), as well as F290Y at pH 4.5 (white), pH 6.1 (cyan), and pH 8.0 (pink). All models were drawn by PyMOL.

Figure 8. Structural interpretation for the hydrolysis of WT and the effective condensation of F290Y

The proposed WT Tyr48/Glu335-related hydrolysis mechanisms of EH2S (A) and EHS (B) in Scheme 2 (Figure 1B) and F290Y catalyzing condensation reaction (C). The hydrogen bonds (dotted lines) and the half bonds (dashed lines) are indicated.

(A)

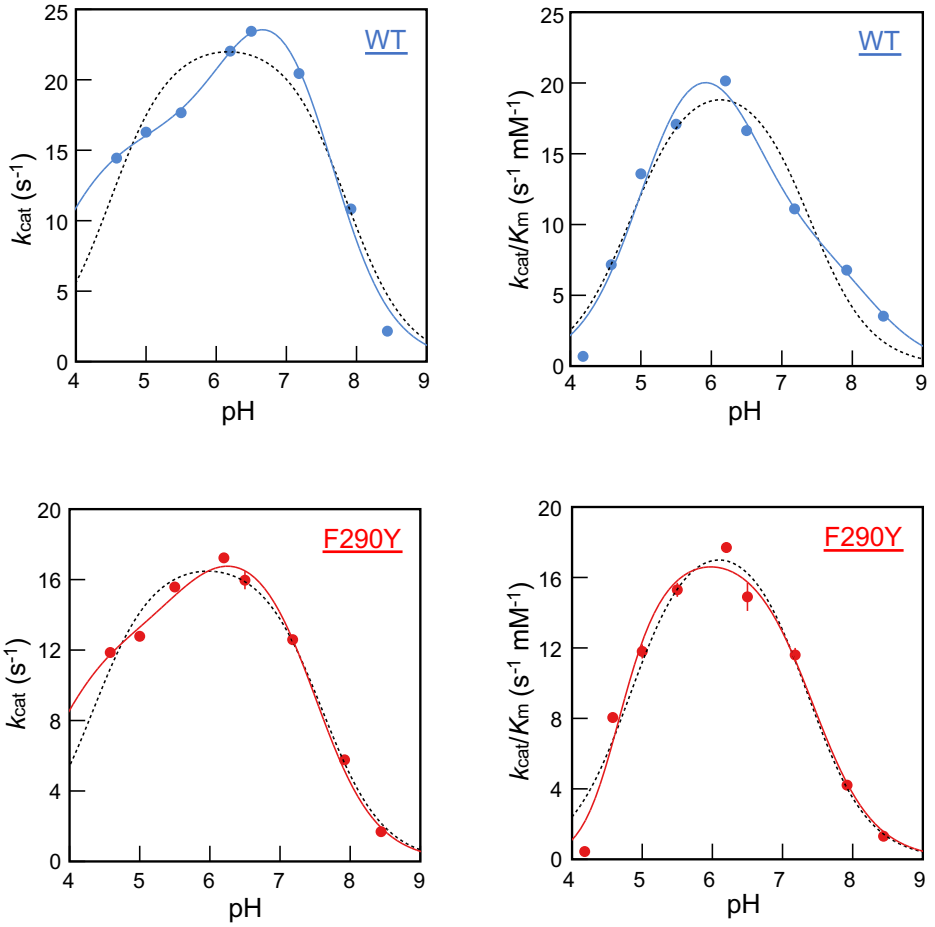

(B)

Scheme 1

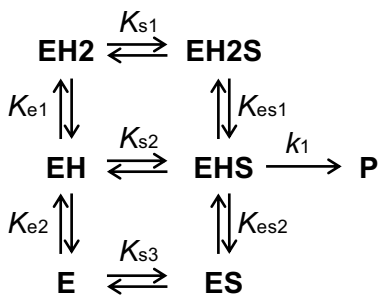

Scheme 2

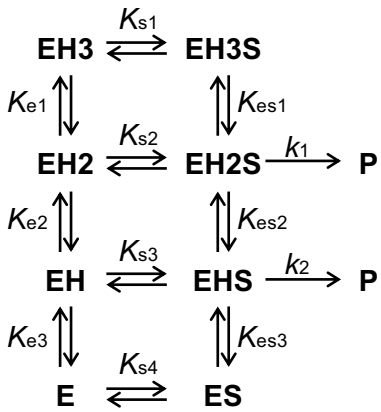

Figure 1

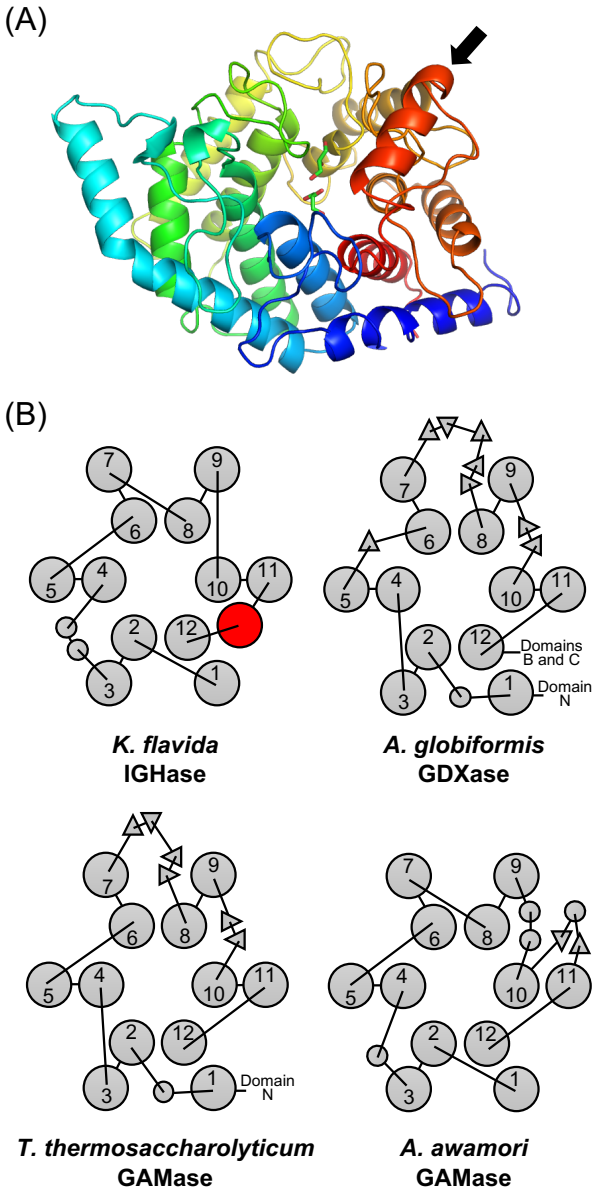
(A)
(B)
7
9
6
8
5
4
10
11
2
12
3
1
Domains B and C
Domain N
K. flavida
IGHase
A. globiformis
GDXase
T. thermosaccharolyticum
GAMase
A. awamori
GAMase

Figure 2

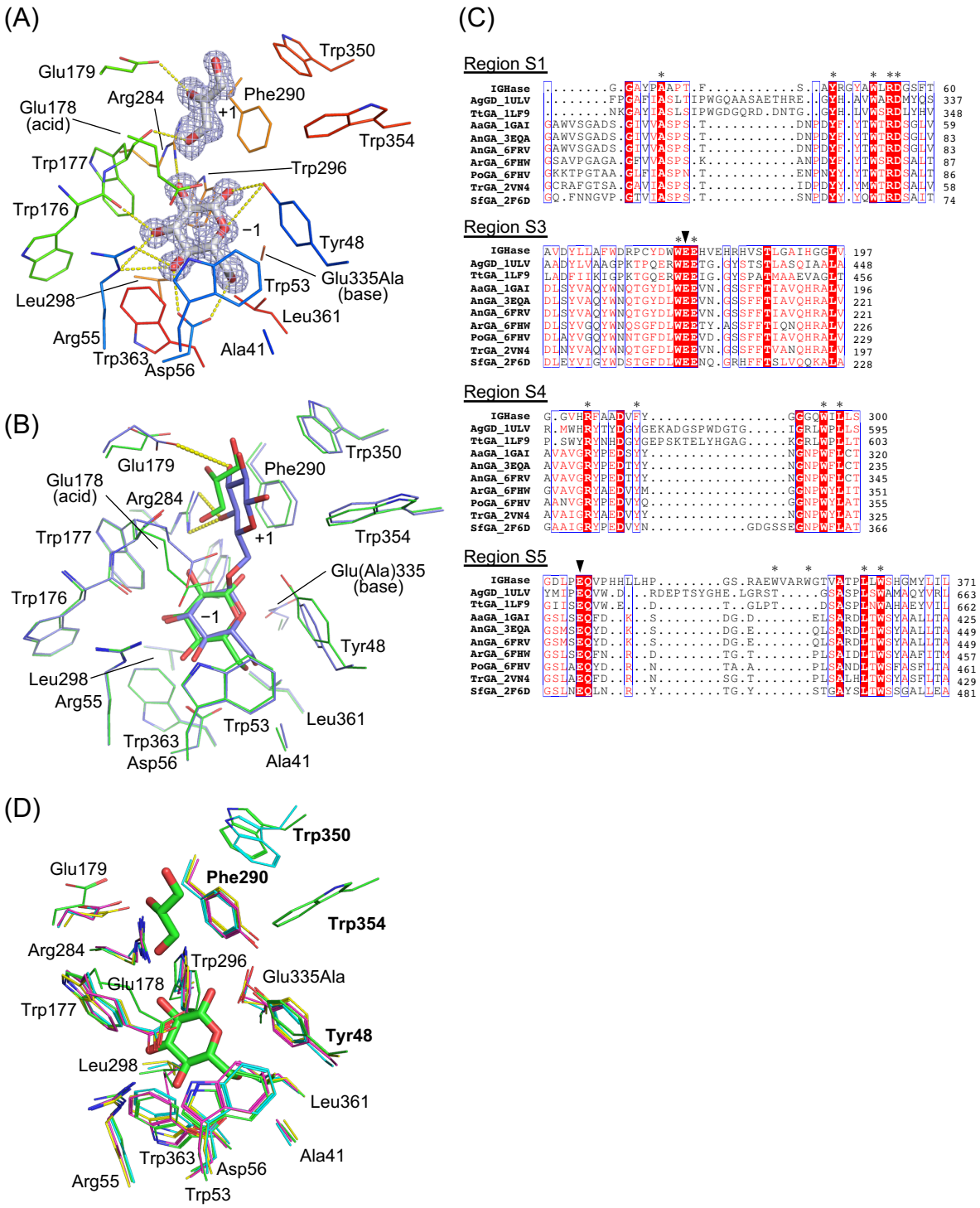
(A)
Trp350
Glu179
Arg284
Phe290
Glu178
(acid)
+1
Trp354
Trp177
Trp296
Trp176
−1
Tyr48
Glu335Ala
(base)
Trp53
Leu298
Leu361
Arg55
Trp363
Ala41
Asp56
(B)
Trp350
Glu179
Phe290
Glu178
(acid)
Arg284
Trp177
+1
Trp354
Glu(Ala)335
(base)
Trp176
−1
Tyr48
Leu298
Arg55
Trp53
Leu361
Trp363
Asp56
Ala41
(C)
Region S1
IGHase .....G.GAYPAAPT.F.....S..AYRGYAWRDGSFT 60
AgGD_1ULV .....FPGAFIASLTIPWGQAASAETHRE..GYH.AVWARDMYQS 337
TtGA_1LF9 .....NKGAYIASLSIPWGDGQRD.DNTG..GYH.LVWSRDLYHV 348
AaGA_1GAI GAWVSGADS.GIVVASPS.T.....DNPDYPF.YTWTRDGGLV 59
AnGA_3EQA GAWVSGADS.GIVVASPS.T.....DNPDYPF.YTWTRDGGLV 83
AnGA_6FRV GAWVSGADS.GIVVASPS.T.....DNPDYPF.YTWTRDGGLV 83
ArGA_6FHW GSAVPGAGA.GPVVASPS.K.....ANPDYPF.YTWSRDGALT 87
PoGA_6FHV GKKTPGTAA.GHFIASPN.T.....ENPNYPY.YTWTRDGALT 86
TrGA_2VN4 GCRAFGTSA.GAVIASPS.T.....IDPDYPY.YMWTRDGALV 58
SfGA_2F6D GQ.FNNGVP.GIVLASPS.T.....SNPDYPY.YQWTRDSALT 74
Region S3
IGHase AVDYLLAFWDRPCYDWEEHVEHRHVSTLGAIHGGLV 197
AgGD_1ULV AADYLVAAGPKTPQERWEETG.GYSTSTLASQIAALA 448
TtGA_1LF9 LADFIIKIGPKTGQERWEEIG.GYSPATMAAEVAGLT 456
AaGA_1GAI DLSYVAQYWNQTGYDLWEEVN.GSSFFTIAVQHRALV 196
AnGA_3EQA DLSYVAQYWNQTGYDLWEEVN.GSSFFTIAVQHRALV 221
AnGA_6FRV DLSYVAQYWNQTGYDLWEEVN.GSSFFTIAVQHRALV 221
ArGA_6FHW DLSYVGQYWNQSGFDLWEETY.ASSFFTIQNQHRALV 226
PoGA_6FHV DLAYVGQYWNNTGFDLWEEVD.GSSFFTIAVQHRALV 229
TrGA_2VN4 DLNYVAQYWNQTGFDLWEEVN.GSSFFAVANQHRALV 197
SfGA_2F6D DLEYVIGYWDSTGFDLWEENQ.GRHFFTSLVQQKALA 228
Region S4
IGHase G.GVHRFAADVFY.....GGGQWILLS 300
AgGD_1ULV R.MWHRYTYDGWGEKADGSPWDGTG.....IGRLWPLLS 595
TtGA_1LF9 P.SWYRYNHDGWGEPSKTELYHGAG.....KGRLWPLLT 603
AaGA_1GAI AVAVGRYPEDSYY.....NGNPWFLCT 320
AnGA_3EQA AVAVGRYPEDTYY.....NGNPWFLCT 235
AnGA_6FRV AVAVGRYPEDTYY.....NGNPWFLCT 345
ArGA_6FHW GVAVGRYAEDVYM.....GGNPWYLIT 351
PoGA_6FHV AANVGRYPEDVYQ.....GGNPWYLAT 355
TrGA_2VN4 AVAIGRYAEDVYY.....NGNPWYLAT 325
SfGA_2F6D GAAIGRYPEDVYN.....GDGSSEGNPWFLAT 366
Region S5
IGHase GDLPEQVPHHLLHP.....GS.RAEWVARWGTVATPLLWSHGMYLIL 371
AgGD_1ULV YMTPEQVW.D...RDEPTSYGHE.LGRST.....GSASPLSWAMAQYVRL 663
TtGA_1LF9 GITSEQVW.E...D.....T..GLPT.....DSASPLNWAHAEYVIL 662
AaGA_1GAI GSLSEQFD..K..S.....DG.D.....ELSARDLTWSYAALLTA 425
AnGA_3EQA GSMSEQYD..K..S.....DG.E.....QLSARDLTWSYAALLTA 449
AnGA_6FRV GSMSEQYD..K..S.....DG.E.....QLSARDLTWSYAALLTA 449
ArGA_6FHW GSLSEQFN..R..D.....TG.T.....PLSAIDLTWSYAAFITM 457
PoGA_6FHV GSLAEQYD..R..N.....TA.A.....PLSANDLTWSFASFLTA 461
TrGA_2VN4 GSLAEQFD..R..N.....SG.T.....PLSALHLTWSYASFLTA 429
SfGA_2F6D GSLNEQLN..R..Y.....TG.Y.....STGAYSLTWSSGALLEA 481
(D)
Trp350
Glu179
Phe290
Trp354
Arg284
Trp296
Glu178
Glu335Ala
Trp177
Tyr48
Leu298
Leu361
Trp363
Asp56
Ala41
Arg55
Trp53

Figure 3

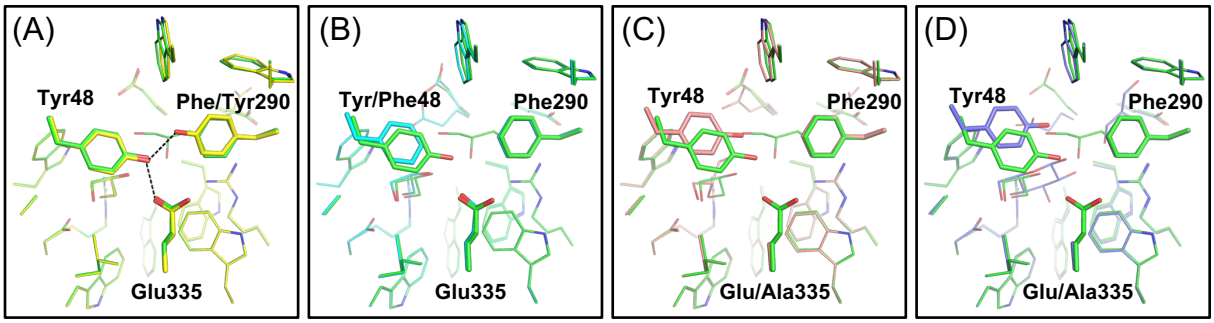
(A)
Tyr48
Phe/Tyr290
Glu335
(B)
Tyr/Phe48
Phe290
Glu335
(C)
Tyr48
Phe290
Glu/Ala335
(D)
Tyr48
Phe290
Glu/Ala335

Figure 4

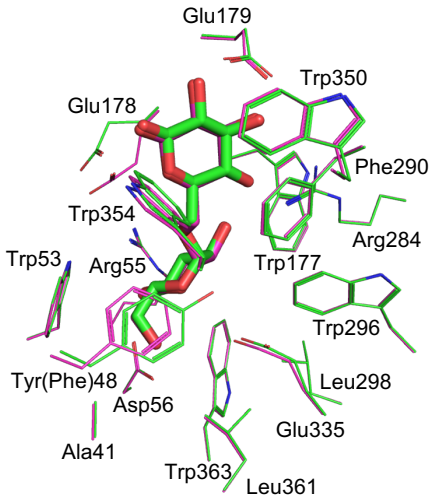
Glu179
Trp350
Glu178
Phe290
Trp354
Arg284
Trp53
Arg55
Trp177
Trp296
Tyr(Phe)48
Leu298
Asp56
Glu335
Ala41
Trp363
Leu361

Figure 5

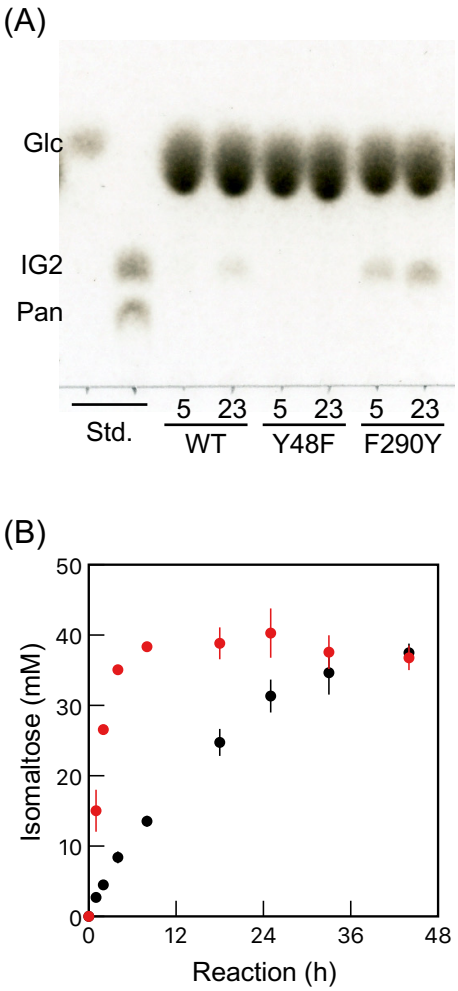
(A)
Glc
IG2
Pan
Std.
5
23
5
23
5
23
WT
Y48F
F290Y
(B)
Isomaltose (mM)
50
40
30
20
10
0
0
12
24
36
48
Reaction (h)

Figure 6

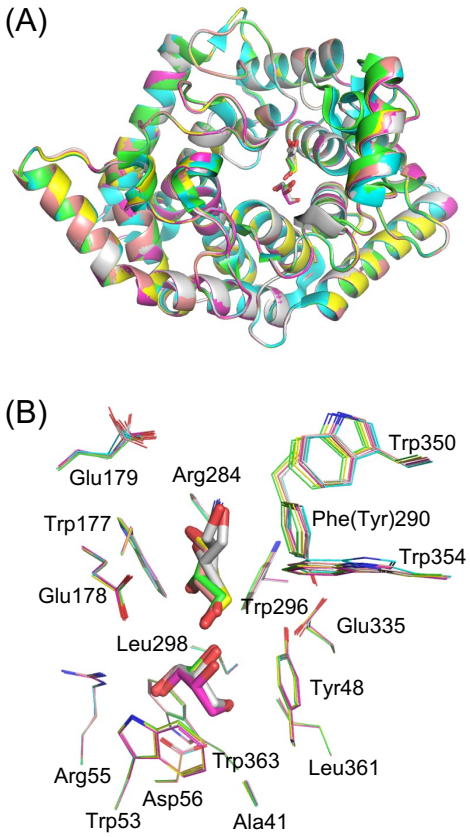
(A)
(B)
Glu179
Arg284
Trp350
Trp177
Phe(Tyr)290
Trp354
Glu178
Trp296
Glu335
Leu298
Tyr48
Arg55
Trp363
Leu361
Asp56
Trp53
Ala41

Figure 7

(A) Hydrolysis by EH2S form of WT

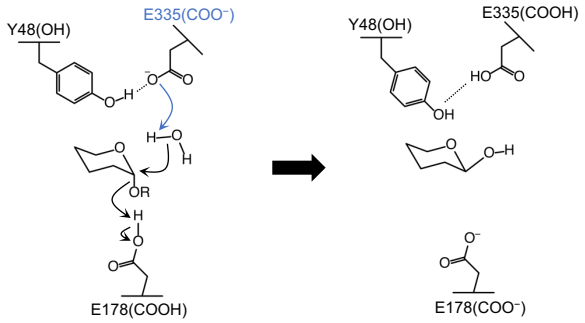

(B) Hydrolysis by EHS form of WT

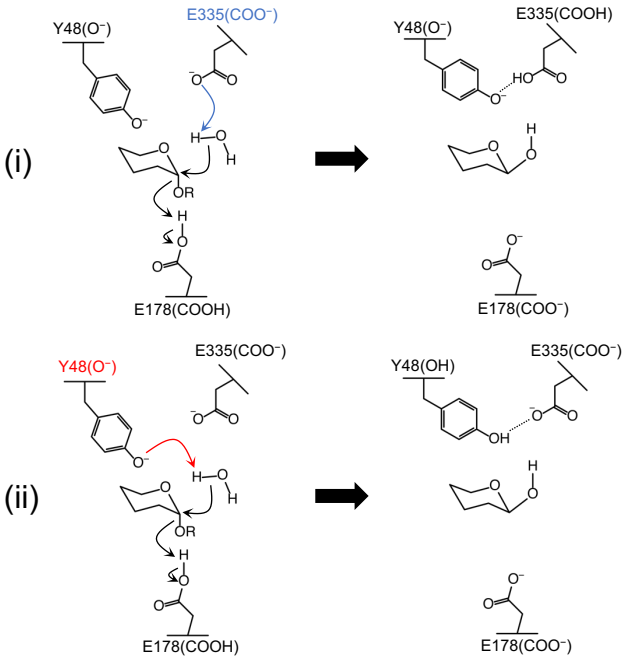

(C) Condensation by F290Y

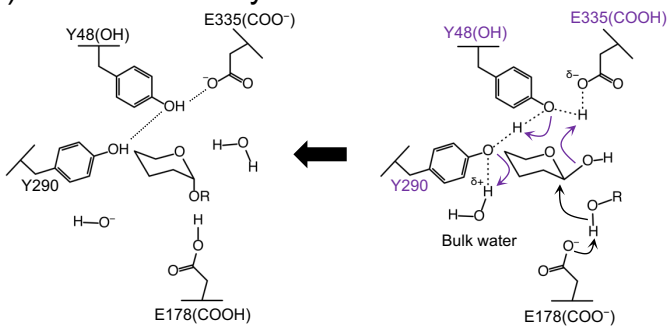

Figure 8